Journal of Energy Storage 66 (2023) 107449

Contents lists available at ScienceDirect

Journal of Energy Storage

journal homepage: www.elsevier.com/locate/est

Research papers

Highly conductive phase change composites based on paraffin-infiltrated graphite panels for photo/electrothermal conversion and storage

Safna Nishad [a], Peter Kasak [a], Igor Krupa [a,b,*]

[a] Center for Advanced Materials, Qatar University, 2713 Doha, Qatar
[b] Materials Science and Technology Graduate Program, College of Arts and Sciences, Qatar University, 2713 Doha, Qatar

ARTICLE INFO

Keywords:
Phase change material
Thermal energy storage
Paraffin
Graphite panel
Energy conversion

ABSTRACT

The extensive utilization of phase change materials (PCMs) for thermal energy harvesting, storage, and thermal management is often constrained by their inadequate thermal and electrical conductivity, form instability, and lack of photoabsorbance. To overcome these challenges, a phase change composite was prepared by vacuum infiltration of paraffin wax (PW) into a highly conductive scaffold of graphite panel (GP). Various PW grades with different phase change temperatures were tested to study their suitability for a wide range of applications. Graphite-based skeleton ensured high thermal and electrical conductivity and impeded liquid PW leakage in all composites. The composite thermal conductivity was enhanced up to 677 and 22 times that of PW in the axial and radial directions, respectively. The latent heat capacity of the composites varied between 88.5 and 102.7 J/g, depending on the PW grade. The composites are capable of harvesting thermal energy either by applying a small voltage of 1.8 V with a high electrothermal conversion efficiency of up to 71.1 % or by simulated sunlight with an excellent photothermal conversion efficiency of up to 76.5 %. The simple fabricating technique, a broad range of applications with different PW grades, and their efficient thermal properties meet the requirements for widespread utilization in thermal energy harvesting, storage, and thermal management of electronics, buildings, etc.

1. Introduction

Nowadays, switching to renewable energy resources is indispensable to reduce the dependence on conventional resources considering their depletion and environmental issues [1,2]. The rapid rise in demand for thermal comfort in the building sector necessitates higher energy consumption for air conditioning, ventilation, and heating systems. Solar energy is the most abundant renewable energy resource that can be either directly utilized for thermal energy or indirectly by photothermal or photovoltaic conversions. However, owing to its intermittent characteristics, solar energy cannot satisfy the continuous energy demand. Phase change materials (PCMs) are ideal candidates for the storage and release of thermal energy as latent heat during its phase change [3,4]. Therefore, excess solar thermal energy and photo-driven energy can be stored during solar irradiation to ensure a continuous energy supply [5]. In addition to solar photothermal conversion, electrothermal harvesting techniques are also important to ensure the reliable utilization of renewable energy sources [6]. During electro-thermal harvesting, Joule heat is generated while the electrons (i.e., electricity) move through an electrical conductor. The excess electricity from the off-peak hours can serve as the source for electro-driven thermal energy harvesting [7]. Moreover, thermal energy harvested from low voltages can be a good choice for the thermal management of electronic devices and batteries in cold regions [8–10]. To ensure the proper functioning of electronic equipment, the thermal management system should consist of a preheater and a heat storage system that should operate at very low voltages [10–12]. Composites of PCMs with superior thermal and electrical conductivity can be used as a preheater and heat storage system [11,13].

Organic PCMs including paraffin wax (PW) are widely being studied due to their thermal and chemical stability, high enthalpy, availability at various melting points, nontoxicity, and low cost [14,15]. Despite these advantages, paraffin has a low thermal conductivity that affects the storage/release rates [16–18]. Moreover, their usage in energy harvesting techniques including photo/electrothermal conversion is limited owing to poor photoabsorption or electrical conductivity [19–21]. The lack of shape stability or leakage of PCMs during melting not only creates compatibility issues but reduces the efficiency by decreasing the latent heat capacity [22–24].

Recently, composite PCMs have been prepared by adding conductive fillers such as carbon nanotubes [16,25,26], graphene oxide [27–29],

* Corresponding author at: Center for Advanced Materials, Qatar University, 2713 Doha, Qatar.
E-mail address: igor.krupa@qu.edu.qa (I. Krupa).

https://doi.org/10.1016/j.est.2023.107449
Received 5 January 2023; Received in revised form 4 April 2023; Accepted 13 April 2023
Available online 26 April 2023

graphite nanoplatelets [16,30,31], expanded graphite [32,33], and carbon nanofibers [34,35] to the PCMs for enhancing the conductivities and photoabsorption. However, the obtained composites exhibited unsatisfactory effective thermal conductivities due to the thermal junction resistances of the nanofillers [36]. For example, the thermal conductivity of PW increased from 0.2 to 3.98 W/m.K by blending with 35 % of Ag nanoparticle-modified expanded graphite [37]. Attaining a conductive percolation network and mitigating the interfacial thermal resistance between nano additives and PCM necessitates a significant proportion of nano additives. However, the thermal energy storage capacity is compromised due to the presence of inactive mass [38–40]. On the other hand, three-dimensional porous networks of foams [20,31,41–43] or aerogels [44–46] as supporting matrices for PCMs provide highly conductive pathways and sufficient PCM loading. Thermal conductivity of 2.6 W/m.K was obtained for 78 % PW infiltrated in expanded graphite foam [47]. However, carbon black-reinforced expanded graphite foam further increased the thermal conductivity to 10.5 and 20.5 W/m.K in the solid and liquid states, respectively [48]. Yang et al. [49] incorporated 89 % of PW into MoS_2-modified melamine foam by vacuum infiltration with exceptional photothermal properties. Wu et al. coated the melamine foam with polydopamine to increase the photothermal conversion of the composite [50]. The photothermal conversion efficiency of 76.1 % was obtained for PW-infiltrated graphite foam [51]. However, these techniques often pose certain disadvantages of PCM leakage due to the uncompacted structure of the scaffold, complex synthesis, high fabrication costs, and limited availability for practical applications [52,53].

Graphite panels (GP) have the advantage of high thermal and electrical conductivity, photoabsorbance, a broad variety of material bulk density, and a large specific area of the pores. GPs are widely used for thermal management applications in solar cells due to their highly conductive and heat-sink properties [54–56]. Its pore characteristics prevent liquid PCM leakage by embedding of PCMs into the micro pores. Although PCM loading in GP will be lower than that of foams, thermal stability can be ensured without any liquid PCM leakage even after several thermal cycles. A wide variety of GPs are available in the market with variable density (0.7–1.8 g/cc), thermal conductivity (150–490 W/m.K in the axial direction and 4.9–5.8 W/m.K in the radial direction) and electrical resistivity (7–15 μΩm in the axial direction and 600–950 μΩm in the radial direction). Depending on the application including space and water heating, thermal management of solar cells, electronics, buildings, etc., PW of various phase change temperatures can be infiltrated into GP.

The high radial thermal conductivity and photoabsorbance of the composite can provide effective photothermal conversion and storage. Moreover, the composite's high axial thermal and electrical conductivity helps to generate and store excellent Joule heat at very low voltages in a short period. The simple fabrication technique and different range of applications made this study different from others.

In this work, we utilize GP as a highly conductive and photoabsorptive framework to accommodate different types of PWs as PCM. The vacuum-infiltrated PW in the micropores of GP relatively reduces the leakage issue even after several consecutive heating and cooling cycles. Furthermore, excellent photo/electrothermal conversion efficiency was determined from the temperature evolution curves.

2. Experimental

2.1. Materials

Graphite panel (GP, SIGRATHERM, SGL Carbon GmbH, Germany, the density of 0.7 g/cm^3, thickness of 2 mm, and porosity of 0.7) and Paraffin Wax (PW, Grade RT35, RT44, RT54, and RT64, Rubitherm Technologies, Germany, the melting point of 35 °C, 44 °C, 54 °C, and 64 °C, respectively) were used for GP_PW composite preparation.

2.2. Preparation of GP_PW composites

The GP_PW composites were formed by vacuum impregnation technique. The particular PW (RT35, RT44, RT54, and RT64) was melted at 100 °C and the GP was completely immersed in the liquid PW and transferred to a vacuum oven at 50 kPa of vacuum for 24 h. Then the GP_PW composites were removed from the oven above its melting temperature and the excess wax around the sample was wiped out using a cotton tissue. The PW loadings on the GP_PW composites coded as GP_RT35, GP_RT44, GP_RT54, and GP_RT64 were determined gravimetrically by measuring the difference in weight before and after vacuum impregnation.

2.3. Characterization

The fracture surfaces of GP and GP_PW composite were obtained by a scanning electron microscope operating at 20 kV (Nova Nano SEM 450). The specimens were immersed in liquid nitrogen for 30 s before breaking to obtain the brittle fracture surfaces of the specimen.

The chemical composition of the samples was analyzed by Fourier-transform infrared spectroscopy (FTIR Spectrometer Frontier, PerkinElmer, USA) using an attenuated total reflectance accessory. The composite scans in the middle infrared region (4000–500 cm^{-1}) were obtained using a ZnSe crystal with a resolution of 4 cm^{-1} at approximately 1.66 pm penetration depth. High spectral quality was ensured by good contact between the sample and crystal using a pressure clamp. The X-ray diffraction patterns of pure PWs and the composites were obtained using a PAN Analytical® EMPYREAN instrument with Cu-Kα radiations. The scan was carried out for 2θ values between 10° and 90° with a step size of 0.01°.

The phase change properties of the PW and GP_PW composites were examined by differential scanning calorimeter (DSC 214 Polyma, NETZSCH-Gerätebau GmbH, Germany) at a heating/cooling rate of 10 °C/min in a nitrogen atmosphere. Thermal cycling analysis was carried out on GP_RT35 composite for 75 cycles at a heating/cooling rate of 10 °C/min using DSC. The thermal stability was determined using thermogravimetric analysis (TGA) and the corresponding first derivative of TGA (DTG) from room temperature to 600 °C with a heating rate of 10 °C/min in a nitrogen atmosphere using TGA 4000 (PerkinElmer, USA) analyzer.

The leakage of the GP_PW composites was determined to characterize the mass loss of PW from 5 × 5 × 0.2 cm samples by gravimetric measurements. The samples were placed in an oven at 80 °C for 2 weeks and measured the weight using an analytical balance, subsequently, the weight loss was calculated according to Eq. (1):

$$\text{Weight loss of PW}(\%) = \frac{(m_i - m_f)}{m_i \times w} \times 100, \quad (1)$$

where m_i is the initial sample mass, m_f is the actual sample mass after 2 weeks in the oven and w is the mass fraction of PW in the composite.

The thermal conductivity of GP and the PCM composites were assessed using a thermal constant analyzer (TCA) with the transient plane source at 21 °C (TPS 2500, Hotdisk, Sweden) with a measurement accuracy of ±3 %. Due to the layered structure of graphite in GP, the thermal conductivity differs for axial and radial directions. The axial thermal conductivity was measured using the slab module in the TCA with 8 cm × 8 cm square samples as shown in Fig. 1a. To measure the radial thermal conductivity, the isotropic module in TCA was used with a cylindrical sample of diameter 6.5 mm (which is equal to the diameter of the TCA sensor used) and 2 mm thick for GP and GP_PW composites as shown in Fig. 1b.

2.4. Photothermal conversion testing

The photothermal conversion test was conducted under simulated

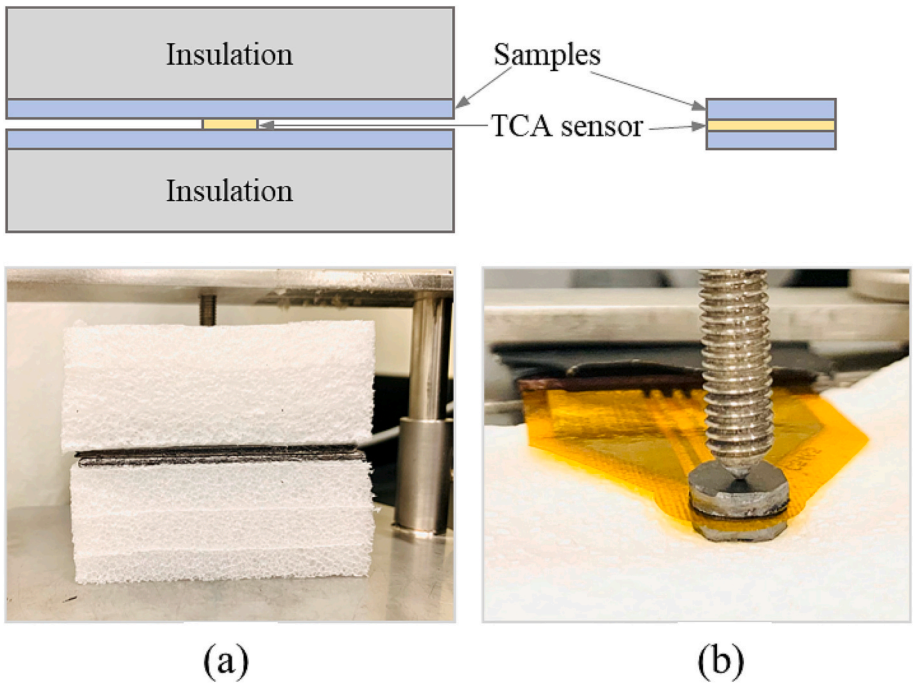

Fig. 1. Schematic (top) and photographic representation of (a) axial thermal conductivity measurement using the slab module, and (b) radial thermal conductivity using the isotropic module in TCA.

irradiation using a solar simulator (Sunlite, ABET Technologies). The GP_PW composites of size 4 × 4 × 0.2 cm were placed inside a foam box and the solar simulator was irradiated under a constant intensity of 1000 W/m^2. The changes in the temperature and heat flux on the sample during the energy conversion and storage process were obtained using a heat flux sensor (Captec, France) and a T-type thermocouple. The data collection and analysis were carried out using a CR1000X datalogger (CampBell Scientific, USA). Fig. 2 shows the experimental setup used for the photothermal conversion test.

2.5. Resistivity measurement and electrothermal conversion testing

The electrical resistivity (ρ) of GP and GP_PW composites were calculated according to Ohm's law while applying a constant voltage through the sample (of size 8 × 2 × 30 mm):

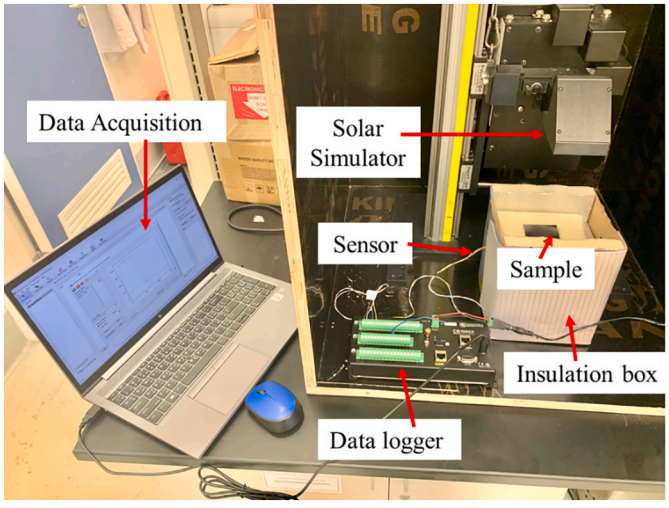

Fig. 2. The experimental setup for the photothermal conversion and storage performance measuring system.

$$\rho = \frac{VA}{IL} \tag{2}$$

where V is the applied voltage, A is the area of the cross-section of the test sample (i.e., 16 mm^2), I is the measured current and L is the length of the test sample (i.e., 30 mm).

The electrothermal conversion testing of the GP_PW composites was conducted on sheet-size samples of 4 × 4 × 0.2 cm as shown in Fig. 3. A certain bias (1.4–2.0 V) was applied to the sample using a DC power supply for a specific time (i.e., 5, 7, or 20 min for different samples). The variation of temperature on the sample surface was measured using a T-type thermocouple during the heating and cooling cycles. The measurements were recorded at 5-sec intervals using a CR1000X datalogger (CampBell Scientific, USA).

3. Results and discussion

3.1. Microstructure of composites

The cross-section of the GP and GP_PW composite specimens has been studied using SEM analysis. Fig. 4 shows the SEM images of the GP and GP_RT44 composite. The GP shows a plate-like structure where flat graphite layers are closely attached to form a sheet with high porosity (i.e., 70 %, estimated from the density calculations). The oxygen functional groups formed between the surface layers of the natural graphite during the exfoliation process resulted in the laminated structure of GP. Although a strong chemical carbon bond exists within the graphite layer, two layers were connected via the van der Waals force. The micropores between the graphite layers are filled by PW during the melt impregnation of PW into GP assisted by vacuum as seen in Fig. 4b.

3.2. Chemical composition

The chemical composition and structural integration of pure PWs and GP were characterized by FTIR spectroscopy. Fig. 5 presents the FTIR spectrum of different PWs and GP_PW composites prepared in this study. The absorption spectra of pure PWs showed asymmetric and

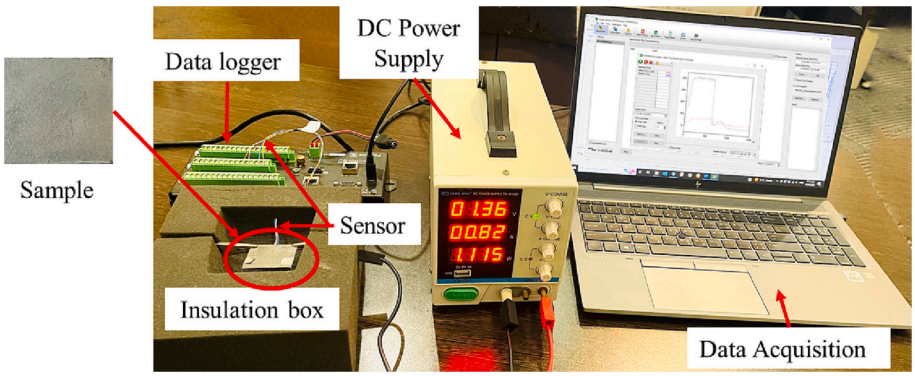

Fig. 3. The experimental setup for the electrothermal energy conversion and storage performance measuring system.

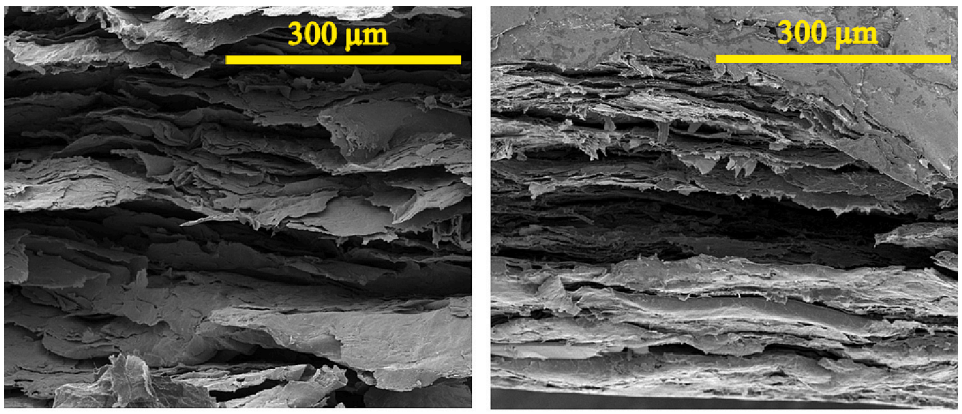

Fig. 4. SEM images of (a) GP, and (b) GP_RT44 composite.

symmetric stretching vibration of aliphatic hydrocarbons at region 2915 and 2848 cm^{-1}, respectively (Fig. 5a). The in-plane vibration of CH_2 and CH_3 are located at 1472 cm^{-1} (1464 cm^{-1} for RT64, 941 cm^{-1} for RT54) and 1370 cm^{-1}, respectively. The rocking vibration of the same group is found at 720 cm^{-1}. In addition to that, an intense absorption peak can be seen for RT54 at 1716 cm^{-1} due to the characteristic C═O stretching vibration of carboxylic groups of fatty acids [57]. Similarly, for RT64, absorption peaks are observed at 3340 and 1064 cm^{-1} corresponding to O—H stretching and C—O vibration, respectively [58]. However, FTIR investigations of the prepared graphite composites were difficult due to their intractability to infrared absorption characteristics [59]. Nevertheless, FTIR of composite samples indicate functional group of PWs after fabrication and incorporation to structure (Fig. 5b).

XRD was further used to characterize pure PWs and GP_PW composites as depicted in Fig. 6. Graphite structure was clearly indicated by peaks at $2\theta = 26.5^{\circ}$ and 54.5° corresponding to planes (002) and (004). Samples with incorporated wax showed diffraction peaks at $2\theta = 21.6^{\circ}$ and 24.0°, which are ascribed to the characteristic monoclinic paraffin-based structures with the (110) and (200) crystal planes, respectively [60].

3.3. Thermophysical properties of composites

The phase change temperature and latent heat of pure PW (i.e., RT35, RT44, RT54, and RT64) and GP_PW composites (i.e., GP_RT35, GP_RT44, GP_RT54, and GP_RT64) were measured using DSC analysis (Fig. 7). Table 1 shows the thermal characteristics of the samples as obtained from DSC. It can be observed from the DSC curves (Fig. 7) that RT44, RT64, and their composites have two endothermic and exothermic peaks during heating and cooling due to the existence of alkanes of different molecular weights. Although the two peaks are close during melting for RT44, RT64, and their composites as seen in Fig. 7a, two distinct peaks are observed during crystallization as shown in Fig. 7b. The solid-liquid transition peak of GP_PW composites (i.e., T_m) was slightly varied from pure PW as shown in Table 1 and Fig. 7a. However, the liquid-solid transition peak (i.e., T_c) was decreased by 2.2–4.6 °C in the composite than pure PW. This reduced phase change temperature of the composites than pure PW is due to the confinement of PW in the microscopic pores of GP, which prevents molecular motion during the phase change process [61]. The reproducibility of the energy storage and release of GP_RT35 composite (as it was the best composite in terms of energy conversion and storage efficiency in this study) was verified by conducting 75 cycles of heating and cooling in DSC as shown in Fig. 8. The variations in phase change temperature and the latent heat are insignificant and the composite is stable after several thermal cycles. Moreover, the FTIR and XRD plots of the GP_RT35 composite look similar before and after thermal cycles confirming the unchanged chemical structure of the composite after cycling.

The latent heat capacities of the composites were significantly reduced from that of pure PW. It is because that GP cannot contribute to the heat storage capacity but rather supports PW and improves thermal conductivity. The discrepancy in the latent heat from the DSC (i.e., ΔH_m) and calculated value from the PW loading (i.e., ΔH_{mcalc}) was due to the uneven distribution of PW in the GP matrix. The macroscopic heterogeneity of the composite will not be accounted for in DSC measurements as the sample size is relatively small (i.e., 5–10 mg). However, all measurements are repeated in triplicates, and the mean and standard deviations are reported in Table 1.

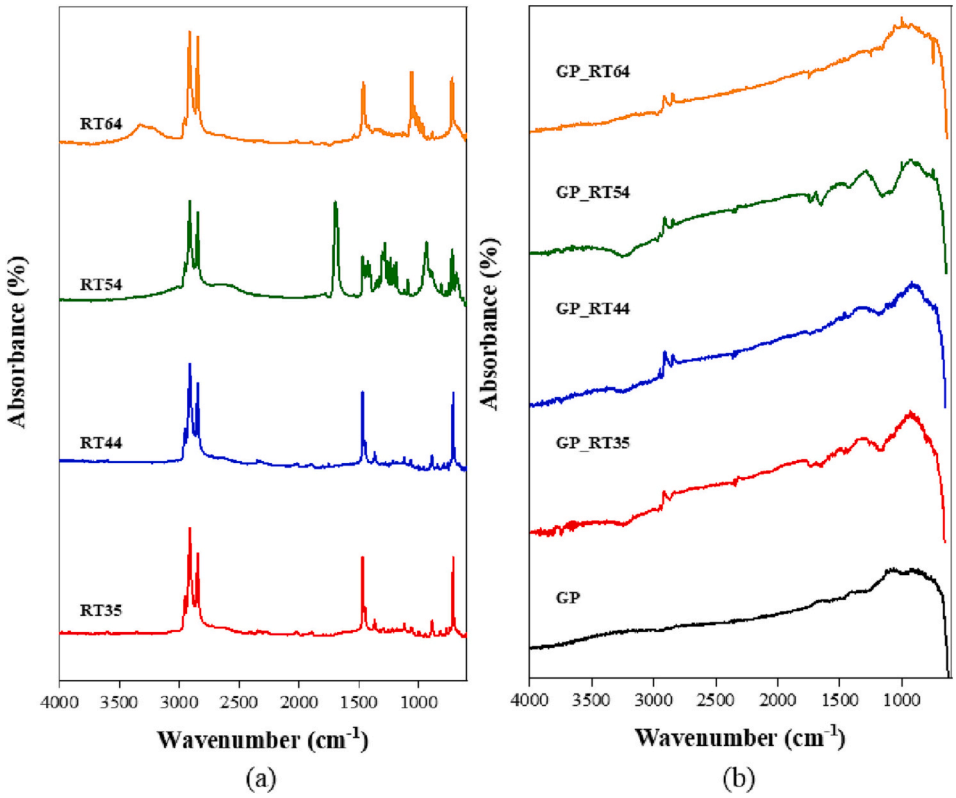

Fig. 5. FTIR spectra of (a) pure PWs, and (b) GP and GP_PW composites.

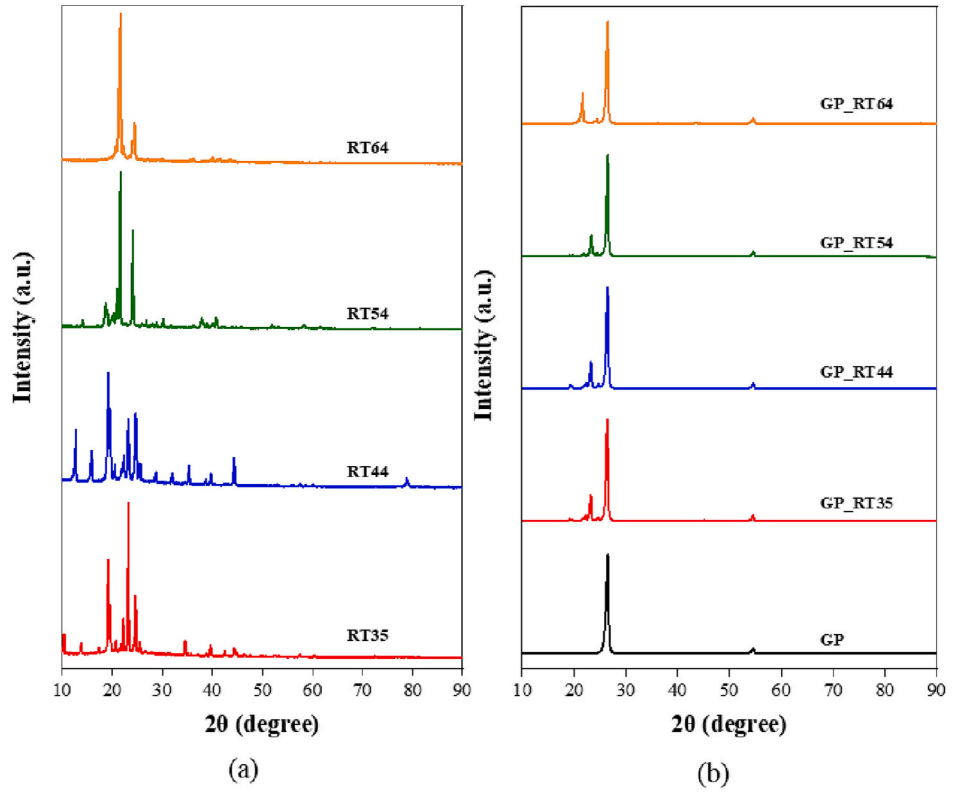

Fig. 6. XRD patterns of (a) pure PWs, and (b) GP and GP_PW composites.

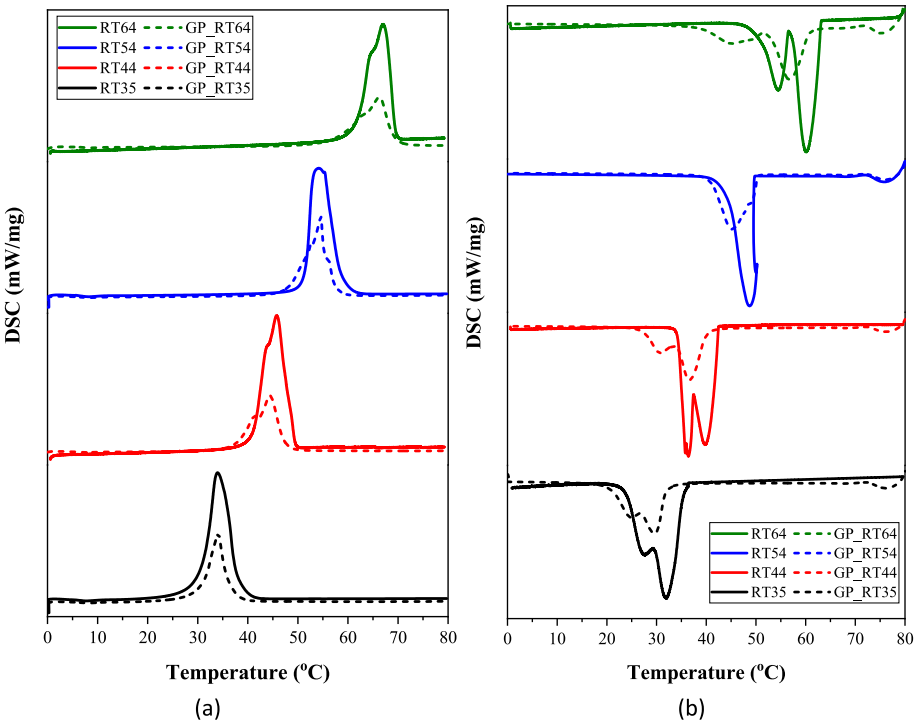

Fig. 7. DSC curves of PW and GP_PW Composite; (a) for heating, and (b) for cooling.

Table 1
Thermal characteristics of PW and GP_PW composites from DSC and latent heat calculated from PW loading.[a]

Sample	Heating		Cooling		PW content from mass calculation (%)	ΔH_{mcalc} (J/g)	Enthalpy efficiency (%) $\Delta H_c/\Delta H_{mcalc}$
	T_m (°C)	ΔH_m (J/g)	T_c (°C)	ΔH_c (J/g)			
RT35	33.9	227.6 (0.2)	31.8	227.4 (0.1)			
GP_RT35	34.1	96.7 (1.6)	29.6	93.4 (1.8)	41.8 (1.4)	95.1	98.2
RT44	45.7	233.4 (0.1)	39.5	231.3 (0.1)			
GP_RT44	44.3	102.7 (1.7)	37.1	101.6 (1.5)	43.8 (1.4)	96.4	105.4
RT54	54.2	192.4 (0.1)	50.5	193.9 (0.1)			
GP_RT54	54.6	88.5 (1.9)	45.9	89.0 (1.8)	43.7 (1.1)	84.1	105.8
RT64	67.0	231.4 (0.2)	60.2	225.9 (0.1)			
GP_RT64	66.3	92.6 (2.0)	57.1	91.8 (1.8)	39.2 (1.0)	88.4	103.8

[a] Standard deviation from three samples is shown in the parenthesis.

The thermal stability of PW and GP_PW composites was evaluated from the TGA curves as displayed in Fig. 9. Pure PWs and their respective composites start to be degraded at the same temperature denoted as $T_{i\text{-}d}$ in Fig. 9b (inset table). 100 % of weight loss occurs at 280 °C and 310 °C for RT54 and RT64 PWs, which is different for their respective composites, as shown in Fig. 9b (inset table, column $T_{f\text{-}d}$). However, RT35 and RT44 exhibited the same temperature range for degradation of PW in their respective composites as given in Fig. 9b, inset table. The total weight loss percentage was obtained as shown in Fig. 9b, which varies negligibly with the mass fraction obtained from the weight calculations.

The form stability is another crucial factor for energy storage applications with PCMs. The leakage of PW from the composite was estimated by the weight loss calculations when placed in an oven at 80 °C in a long-term heating stress experiment for two weeks. Importantly, the results show that the composites exhibited only a negligible leakage of 2.5 % of PW after two weeks. Fig. 10 shows the images of the composite before and after the leakage test (after 14 days). As the PW leakage was very small, no traces of melted PW were visible on the tissue paper even after 14 days of heating in the oven. In this case, the dense graphite panel accommodates the melted PW and inhibits the massive leakage of PW by the capillary force in the micropores and van der Waals attraction between GP and PW. Therefore, the results from the long-term thermal stressed condition and cyclic DSC test indicate the thermo-physical stability of GP_PW.

3.4. Thermal conductivity and electrical resistivity

Thermal conductivity is a crucial parameter that influences the thermal transfer rate for practical applications. The thermal conductivity of pure PW was very low (i.e., 0.20 W/m.K), whereas the supporting GP has a different thermal conductivity in the axial (i.e., 142.4 W/m.K) and radial (i.e., 5.55 W/m.K) directions. Therefore, the GP_PW composites also exhibited different thermal conductivity values in both directions. In this study, the photothermal conversion efficiency is affected by the radial thermal conductivity whereas electrothermal conversion efficiency was influenced by the axial thermal conductivity. Therefore, both the thermal conductivities were measured using TCA for each composite and the findings are given in Fig. 11a. The axial and radial thermal conductivities of the GP_PW composites varied in the range 134.2–136.1 W/m.K and 4.32–4.41 W/m.K, respectively, which is 677 and 22 times more than the thermal conductivity of pure PW. On the other hand, the introduction of PW reduced the thermal conductivity of GP by 5 % and 21 % in the axial and radial directions, respectively. The

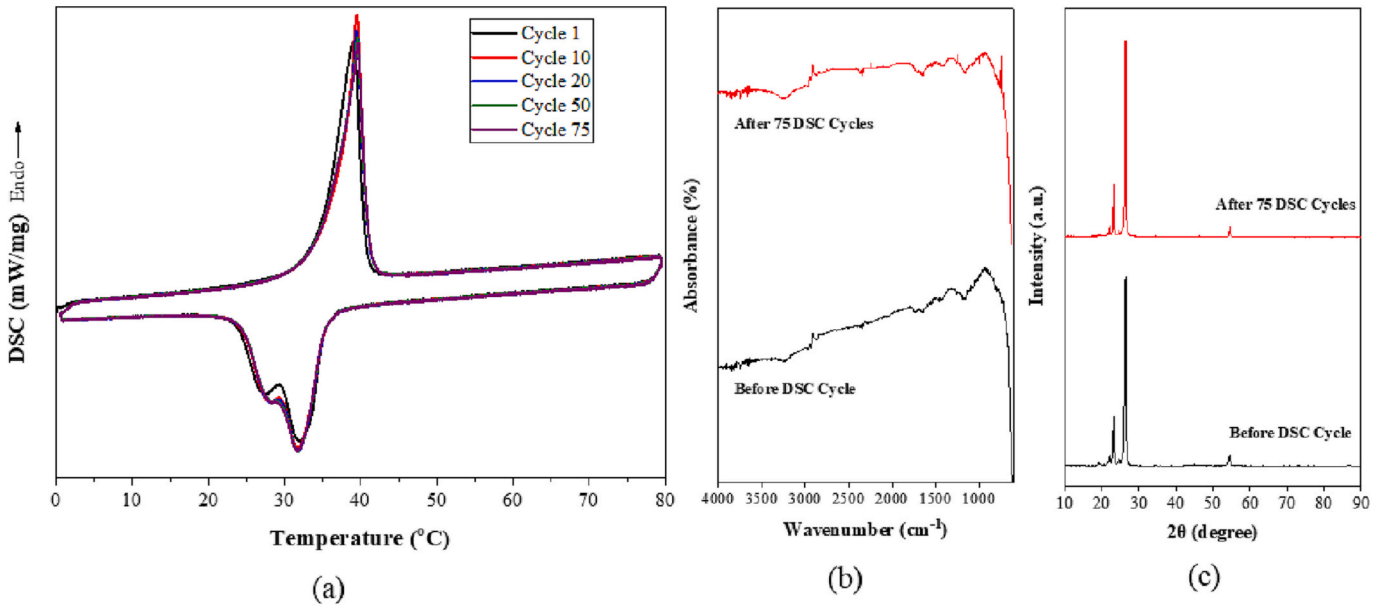

Fig. 8. Thermal cycle results for GP_RT35 (a) DSC curves, (b) FTIR spectra, and (c) XRD pattern of samples before and after DSC thermal cycles.

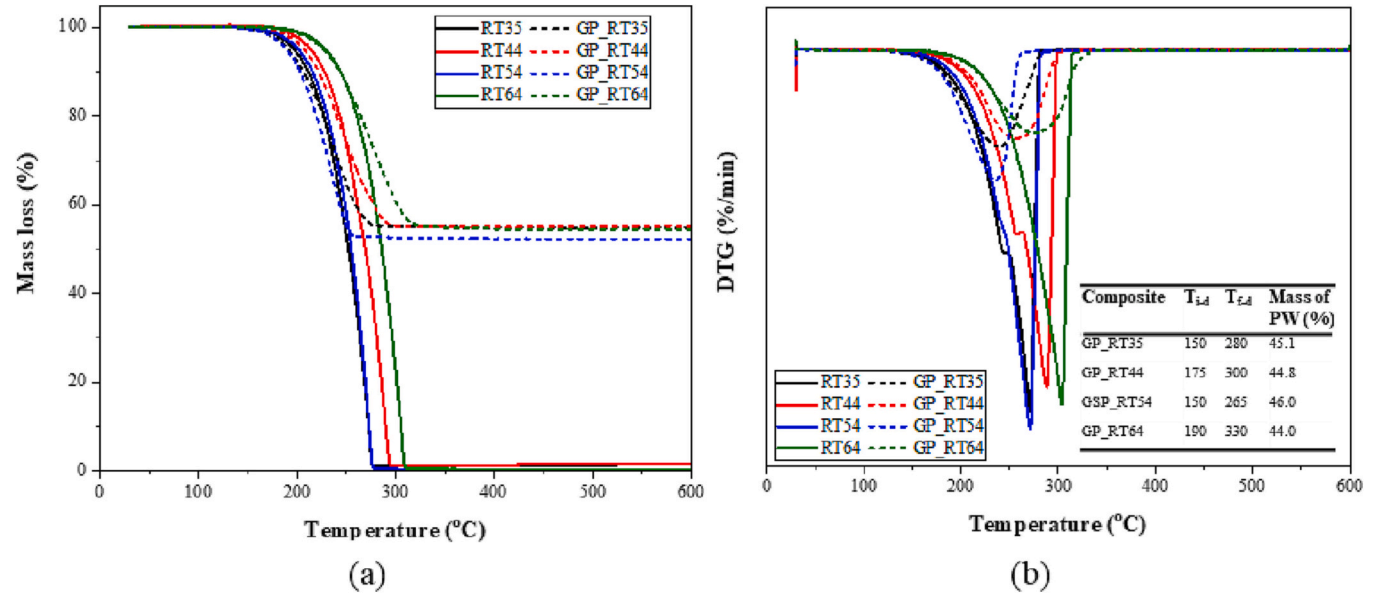

Fig. 9. (a) TGA, and (b) DTG curves for the PWs and GP_PW composites.

thermal conductivities of the composites in this study were very high compared to the previously reported PW-based composite PCMs in Table 2. Therefore, the GP_PW composites improve the thermal transfer during the photothermal and electrothermal conversion process compared to pure PW.

The electrical resistivity of the GP_PW composites was tested by applying different voltages (i.e., 0.15–1.5 V) and measuring the current in the sample (of size 8 × 2 × 30 mm) using a DC power supply (Eq. (2)). The mean and standard deviations of resistivity for GP and GP_PW composites are shown in Fig. 11b. The plots for applied voltage and corresponding measured current for GP and GP_PW composites are provided in Fig. S1 in the Supplementary material. The resistivity of GP was very low (0.84 mΩ.m), suggesting that GP is highly conductive to electricity. The impregnation of PW in GP increased the resistivity of the composite by 2.15–2.65 times that of GP.

3.5. Photothermal conversion

Fig. 12 shows the heat flux and temperature-time plots of GP and GP_PW composites of size 4 × 4 cm^2 (i.e., GP_RT35, GP_RT44, and GP_RT54) under the simulated solar irradiation of 1000 W/m^2 for 20 min. The heat flux and temperatures below the sample were recorded using a heat flux sensor and a T-type thermocouple equipped with a data logger. The sample was placed in an insulation box where the heat loss can be neglected except through the top surface of the sample.

As indicated in Fig. 12a, the temperature of GP increases rapidly with time during solar irradiation and attains a steady state temperature of around 64 °C after 5 min of exposure. The heat flux passing through the samples increases rapidly with time at the beginning of solar irradiation due to a rapid rise in temperature (Fig. 12). The heat flux evolution of GP shows that the heat transfer gradually decreases from the peak due to the convective heat transfer to the air on the sample top surface and reaches

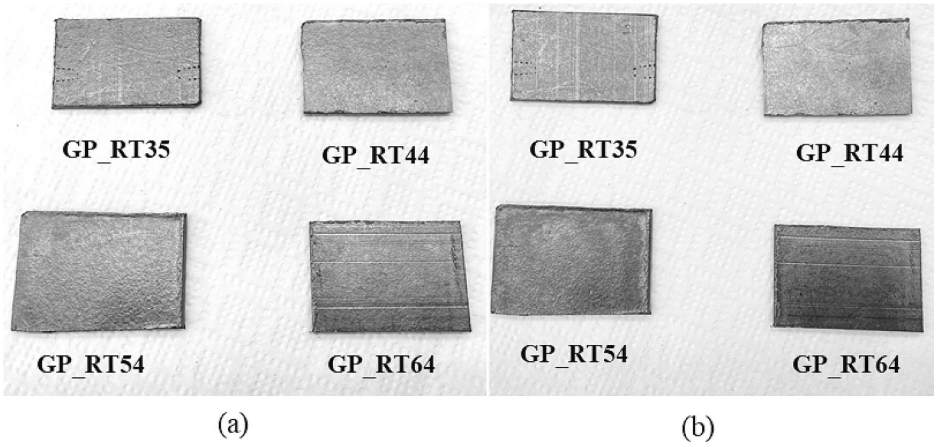

Fig. 10. The images of the composites (a) before and (b) after the leakage test.

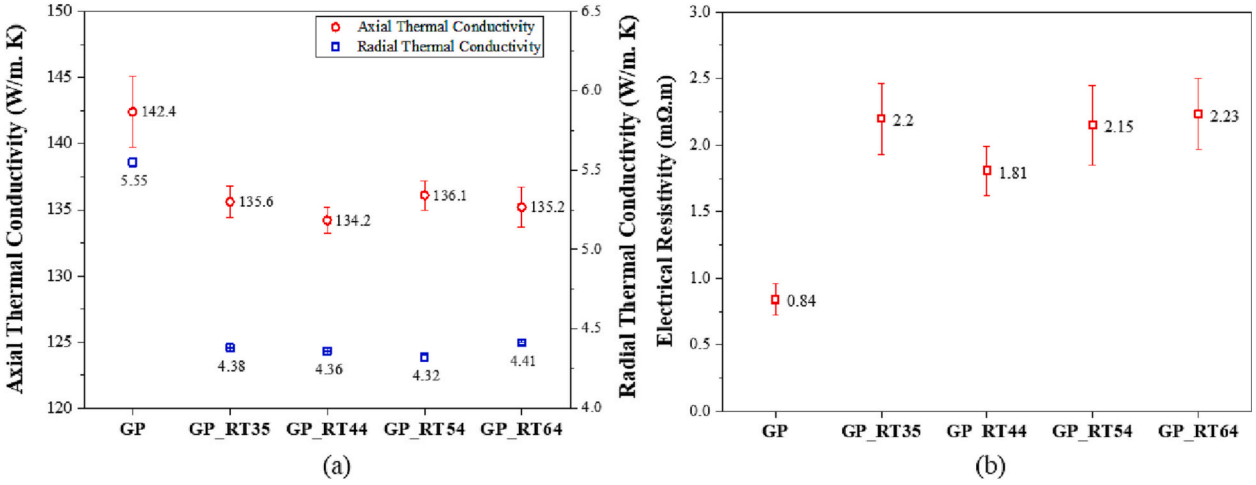

Fig. 11. (a) The axial (empty circle) and radial (empty square) thermal conductivity, and (b) axial electrical resistivity of GP and GP_PW composites.

a steady-state condition. However, for GP_PW composites, the heat flux decreases from the initial peak indicating the start of phase change. The conductive heat flux passing through the composite during this time is partially absorbed for the melting of PW, decreasing the temperature rise. Therefore, a temperature plateau was observed for GP_PW composites near the melting temperature as seen in Fig. 12a. While PW completes melting, the heat flux also increases and attains a steady state as in the case of GP. The fluctuations or noises associated with the heat flux measurements are ascribed to the impact of the surrounding air on the sample top surface.

The photothermal conversion and storage efficiency (η_p) were calculated by the ratio of the latent heat of the paraffin (i.e., the mass of the composite (m) times its enthalpy (ΔH)) to the energy of simulated solar light during a phase change (i.e., the product of the intensity of applied light source (P), the exposed surface area of the sample (S) and time taken for phase change (Δt)). Therefore, the storage efficiency is,

$$\eta_p = \frac{m\Delta H}{PS\Delta t} \tag{3}$$

considering all the paraffin in the composite took part in the phase change.

The calculated efficiencies of the composites under similar experimental conditions are given in Table 3. The efficiency was decreased from 76.5 % to 31.3 % with an increase in phase change temperature (i.e., GP_RT35 > GP_RT44 > GP_RT54 > GP_RT64) due to the increase in time taken for phase change as shown in Fig. 12. This could be due to the increased convective heat loss from the sample surface with an increase in temperature. Therefore, the convective heat loss during the phase change process for GP_RT64 will be higher compared to GP_RT35 and thereby increase the time required to complete the phase change. The photothermal conversion efficiency of GP_RT35 was comparable with PW-based PCM composites reported in previous literature (Table 2) and are promising candidates for solar energy storage systems.

Once the light was off, a rapid drop in temperature was observed for GP. However, for GP_PW composites a gentle decrease in temperature indicates the sensible thermal energy release followed by latent heat release as indicated by the temperature plateau in Fig. 12a. The duration for temperature plateau for GP_RT64 composite was significantly less than other composites due to the convective energy loss. The two exothermic peaks of GP_RT64 and GP_RT44 were clear in the cooling curve, while for GP_RT35 it was difficult to identify as the latent heat release by the composite was not complete in Fig. 12. The two crystallization peaks of the composites GP_RT64, GP_RT44, and GP_RT35 were also observed in DSC curves (Fig. 7) due to the existence of alkanes of different molecular weight.

The repeatability of the measurements was validated through 10 cycles of heating and cooling by the solar exposure and the heat flux and temperature-time evolutions show negligible variation as shown in Fig. 13.

Table 2
Comparison of thermal properties of PW-based PCM composites reported in the literature with this work.

Supporting materials of PW	Thermal conductivity (W/m. K)	Latent heat (J/g)	Photothermal conversion efficiency (%)	Reference
Modified melamine foam/graphene	0.59	130.61	79.4	[62]
Oxygen-deficient TiO_2/reduced GO aerogel	1.22	140.2	89.9	[63]
Carbon foam	–	221.1	67.4	[64]
Modified blast furnace slag	0.25	36.4	–	[65]
Reduce graphene oxide/zirconium carbide co-modified melamine sponge	0.62	137.2	81	[66]
Reduced graphene oxide sponge	0.25	143	88.7	[67]
Melamine foam/ graphene oxide/ graphene nanoparticles	1.46	155.5	88	[68]
Expanded graphite/carbon black	5.77 (solid) 10.54 (liquid)	142.6	60.1	[48]
Expanded graphite/ thermoplastic elastomer	2.2	145.5	72	[69]
Copper foam/ reduced graphene oxide	1.13	111.5	86.7	[70]
Polyolefin elastomer/ expanded graphite	1.413	126.7	58.2	[71]
Graphite panel	4.4 (radial) 135.6 (axial)	96.7	76.5	This work

3.6. Electrothermal conversion

The performance of electrothermal conversion of the GP_PW composite was evaluated in this work by applying a certain bias across the sample. Excellent Joule's heat was generated in the composite when a steady voltage of 1.2–2.0 V is applied for a certain time (i.e., 4, 7, 20 min) due to its high electrical conductivity. The temperature evolution with time for GP and GP_PW composites is shown in Fig. 14.

A rapid increase in temperature was observed in the samples due to the fast response of GP for electrothermal conversion. After 4 min of exposure to constant voltage, GP raised the temperature from 58 °C to 116 °C with an increase in voltage from 1.2 V to 2.0 V. Since the produced heat is not stored by GP (i.e., the specific heat capacity of GP is very low, 0.75 J/g.°C), the sample temperature decreased rapidly once the voltage ceased. However, the PW in the GP_PW composites can store the generated heat as sensible and latent heat. A temperature plateau observed for GP_PW composites near the melting temperature indicates the phase change of PW and latent heat storage as seen in the curves of Fig. 14b–e. The GP_PW composite stored the heat before and after the phase change as solid and liquid sensible heat, respectively. The temperature increases with the applied voltage, and the generated thermal energy was stored as sensible and latent heat by the PW. Although the latent heat stored at different voltages is constant, the time required to complete the phase change decreases with the increase in voltage due to the reduction in the convective energy losses to the surroundings. Since a voltage bias of 1.2 V requires more time to complete the phase change of PW, the experiments for GP_PW composites were conducted for 1.4 V, 1.6 V, 1.8 V, and 2.0 V.

The electrothermal conversion and storage efficiency (η_e) of the composite are computed from Eq. (4).

$$\eta_e = \frac{m\Delta H}{VI\Delta t}, \tag{4}$$

where V is the applied voltage, and I is the measured current. The calculated electrothermal conversion efficiencies of each composite at different voltages are presented in Fig. 15a and Tables S1–S4 (Supplementary material). The electrothermal conversion efficiency of the GP_RT35 composite at 1.8 V was comparable with other PW-based composites reported in the literature (Table 4).

After the constant voltage ceased, the stored sensible and latent heat were released as indicated by the temperature evolution curve. Depending on the amount of liquid sensible storage, the crystallization of PW initializes at different times for the same composite heated at different voltages. For instance, the crystallization of GP_RT35 composite starts at 695, 815, and 910 s for 1.4, 1.6, and 1.8 V voltage biases

Table 3
Photothermal conversion and storage performance of GP_PW composites.

Composites	GP_RT35	GP_RT44	GP_RT54	GP_RT64
Phase change duration (s)	300	450	655	760
Input energy (J)	480	720	1048	1216
Stored energy (J)	368	400	372	380
Energy storage efficiency (%)	76.5	55.6	35.5	31.3

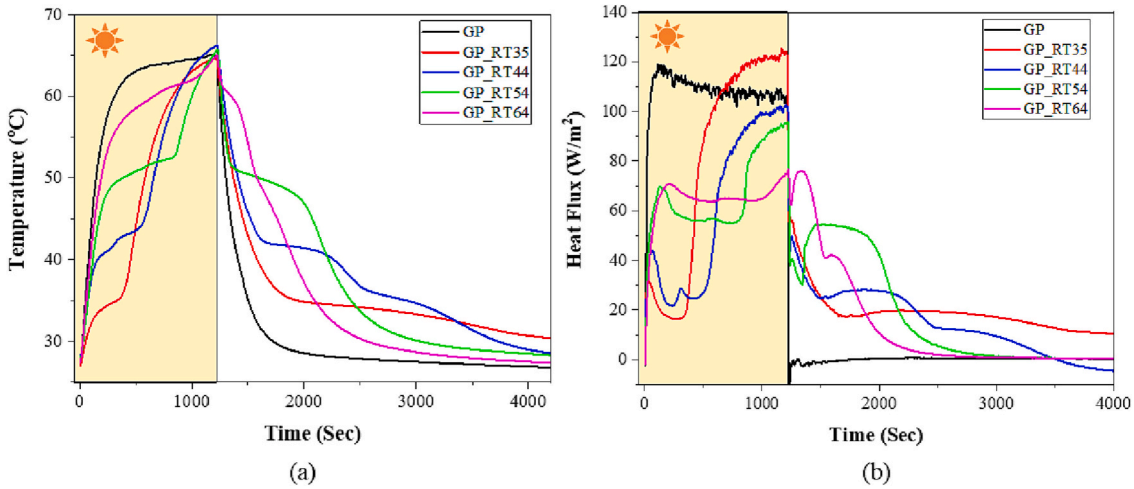

Fig. 12. (a) Temperature-time evolution curves and (b) heat flux-time evolution curves of GP and GP_PW composites during photothermal conversion study.

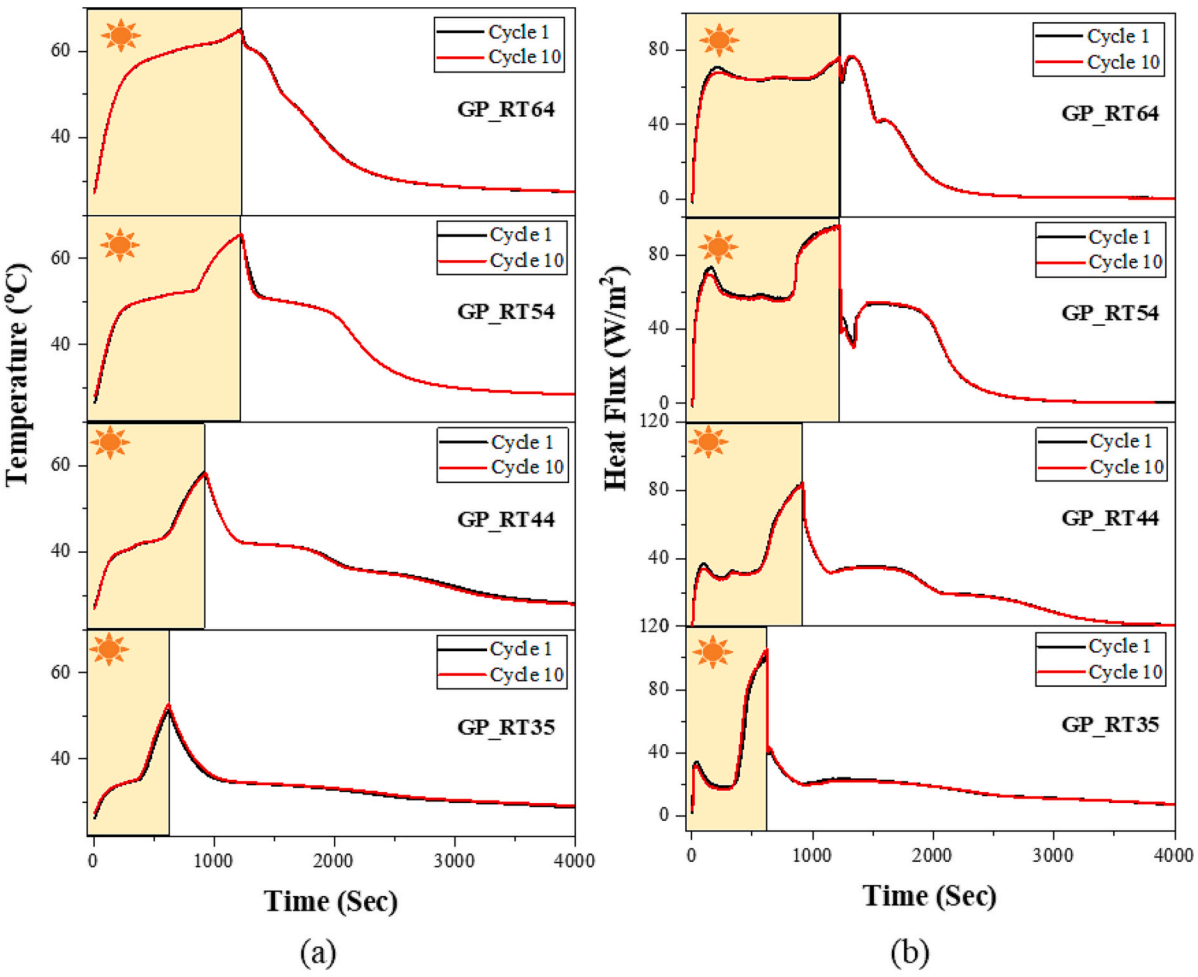

Fig. 13. (a) The temperature and (b) heat flux-time evolution curves of GP and GP_PW composites tested at 10 cycles of heating and cooling during the photothermal conversion study.

as the maximum temperatures were 47.5, 60.5, and 72.5 °C, respectively. However, the time taken for liquid-solid phase change remains the same for each composite at different voltage biases. The two exothermic peaks for GP-RT35, GP_RT44, and GP_RT64 are observed from the two temperature plateaus in the cooling curve. As the endothermic peaks are closer and the solid-liquid phase change occurs faster, two plateaus are not observed in the heating curve of GP_RT44 and GP_RT64. As observed from Fig. 14b–e, the composites can maintain a constant temperature for a long period during cooling compared to heating indicating their effectiveness for thermal management. The total time required to complete solid-liquid and liquid-solid phase change for each composite at different voltages is given in Table 5. As given in Table 5, the composite GP_RT35 requires 130 s to complete phase change at 1.8 V. After the voltage ceased, the composite can remain in the temperature range of 35–27 °C for 1820 s. Similarly, the cooling and electrical heating time for other composites are given in Table 3. Although the heating and cooling time includes the convection heat loss, it is more prominent during cooling. Therefore, the actual time for phase change was estimated by subtracting the time for convective heat transfer, which was determined from Newton's law of cooling (Supplementary material).

The effectiveness of GP_PW composites for thermal management was evaluated by estimating the ratio of cooling time and electrical heating time as given in Fig. 15b. The results show that the time for cooling is 1.2–11.2 times more compared to the time required for electrical heating. On other hand, a small voltage (1.4–2.0 V) applied on GP_PW composites for a short period can maintain the required temperature for a long time. Therefore, the composites are effective in the thermal management of electronic devices in cold regions to maintain the working temperature by electrical heating. However, the cooling time can vary with the type of composite and the ambient temperature.

4. Conclusions

The GP_PW composites with excellent thermal conductivity and photo/electrothermal energy conversion ability were fabricated by vacuum infiltration of PW into GP. The performance of composites was evaluated with PWs of different phase change temperatures to study their suitability in various applications. The capillary and van der Waals attraction forces among the GP and PW prevent the leakage of PWs from the pores of GP. The thermal conductivity of the composite was increased up to 677 and 22 times that of pure PW in the axial and radial directions, respectively, with exceptional thermal conductivity for PCM materials. Excellent photoabsorbance and radial thermal conductivity of the composites provided higher photothermal conversion efficiency. The higher axial thermal and electrical conductivity of the composite enhanced the electrothermal conversion efficiency. However, the efficiency decreases with the increase in the phase change temperature due to the convective energy loss from the composite surface. The composites exhibited excellent thermal cyclic as well as long-term thermal stress stability. The latent heat capacity of the composites varied between 88.5 and 102.7 J/g. The photo and electrothermal conversion efficiencies of the GP_RT35 composite were 76.5 % and 71.1 % at 1.8 V, respectively. The simple fabricating technique, the applicability of different PWs of

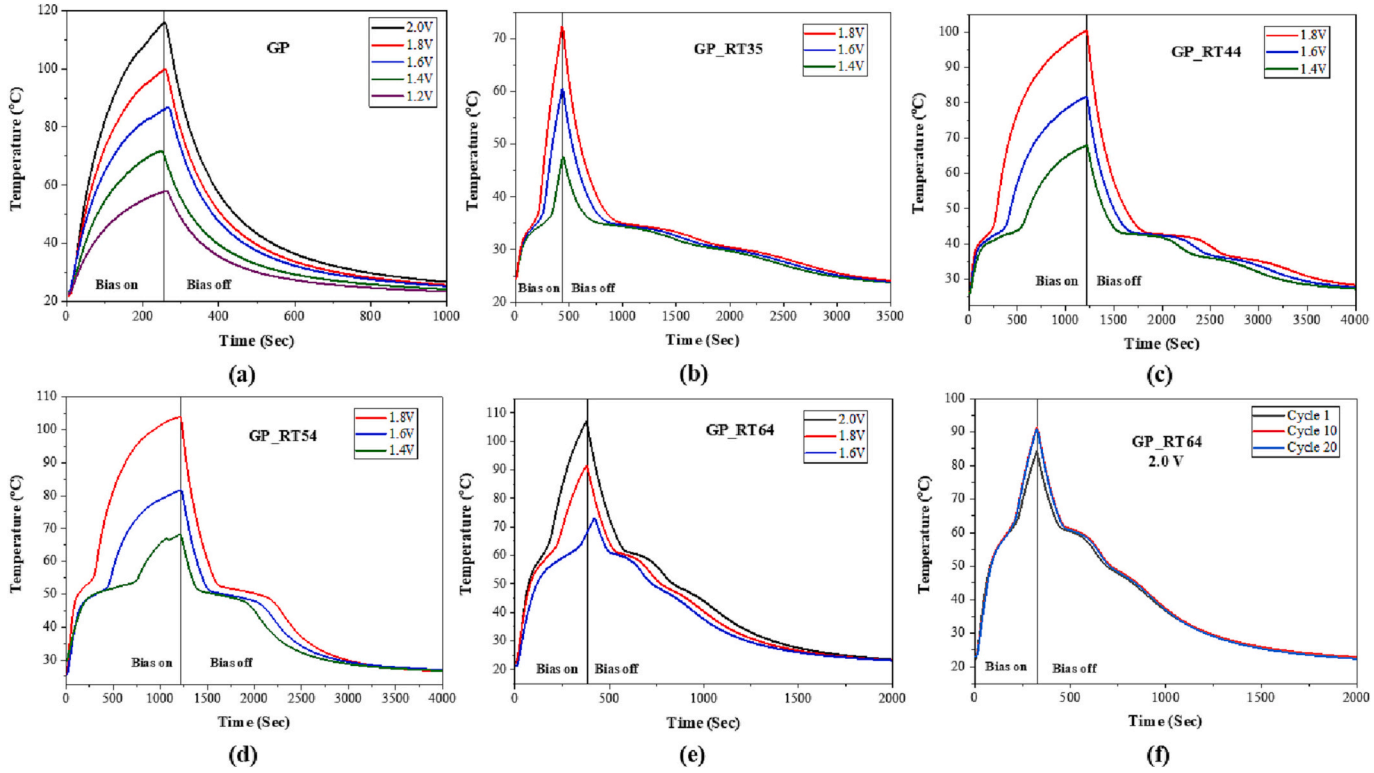

Fig. 14. Temperature-time evolution curves for (a) GP, (b) GP_RT35, (b) GP_RT44, (b) GP_RT54, (b) GP_RT64 at constant voltages of 1.4, 1.6, 1.8, and 2.0 V and (b) GP_RT64 at 2.0 V for 20 cycles during electrothermal conversion study.

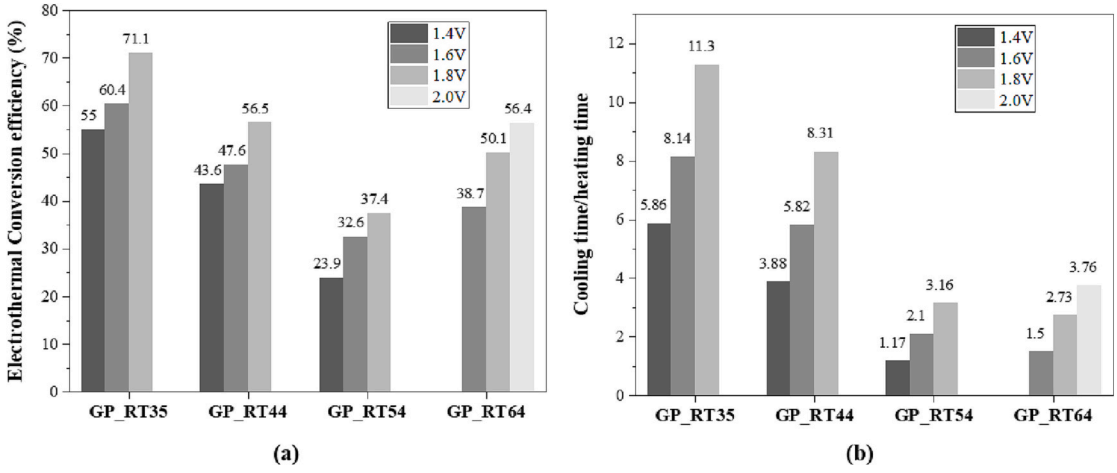

Fig. 15. (a) The electrothermal conversion efficiencies of the GP_PW composites at different voltages, (b) The effectiveness of GP_PW composites for thermal management in terms of the ratio of cooling time and electrical heating time.

Table 4
Comparison of electrothermal conversion performance of PW-based PCM composites reported in the literature with this work.

Supporting materials of PW	Thermal conductivity (W/m.K)	Latent heat (J/g)	Electrothermal conversion efficiency (%)	Voltage (V)	Ref.
Biomass-derived 3D carbon scaffold	0.53	182.2	81.1	3.0	[72]
Melamine foam/graphene oxide/graphene nanoplatelet	1.46	155.5	62.5	2.9	[68]
Graphite foams	1.38	209.2	74.6	5.0	[51]
Carbon cloth	–	93.6	67.4	4.0	[73]
Graphitic carbon foam	–	120.2	74.0	3.6	[21]
Carbon aerogel	–	115.2	71.4	15.0	[74]
Graphite panel	4.4 (radial) 135.6 (axial)	96.7	71.1	1.8	This work

Table 5
The time required for phase change for GP_PW composites at different voltages during heating and cooling.

	Heating				Cooling		
	Time required for phase change (s)				Time for phase change (s), Fig. 14	Temperature range (°C)	Actual time for phase change (s)
Composite	1.4 V	1.6 V	1.8 V	2.0 V			
GP_RT35	250	180	130	–	1820	35–27	1465
GP_RT44	300	200	140	–	1375	43–34	1163
GP_RT54	430	240	160	–	580	52–47	505
GP_RT64	–	200	110	80	500	62–40	300

various phase change properties, and their efficient thermal properties suit them for a wide variety of applications in thermal storage, thermal management of electronics, buildings, etc.

CRediT authorship contribution statement

Safna Nishad: Conceptualization, Methodology, Investigation, Formal analysis, Data curation, Validation, Writing – original draft. **Peter Kasak:** Methodology, Resources, Supervision, Writing – review & editing. **Igor Krupa:** Conceptualization, Methodology, Validation, Resources, Supervision, Project administration, Funding acquisition, Writing – review & editing.

Declaration of competing interest

The authors declare that they have no known competing financial interests or personal relationships that could have appeared to influence the work reported in this paper.

Data availability

Data is contained within the article.

Acknowledgment

SEM was accomplished in the Central Laboratories Unit, Qatar University. The authors greatly acknowledge Dr. Zubair Ahmad (Qatar University) for providing the solar simulator. Authors thank Dr. Patrik Sobolciak and Abdul Jaleel (Qatar University) for their assistance in the experiments. Open Access funding provided by the Qatar National Library.

Funding

This research was funded by the Qatar National Research Fund (a member of The Qatar Foundation), grant number NPRP13S-0127-200177.

Appendix A. Supplementary data

Supplementary data to this article can be found online at https://doi.org/10.1016/j.est.2023.107449.

References

[1] S. Chu, A. Majumdar, Opportunities and challenges for a sustainable energy future, Nature 488 (2012) 294–303, https://doi.org/10.1038/nature11475.
[2] N.S. Lewis, Toward cost-effective solar energy use, Science 315 (2007) (1979) 798–801, https://doi.org/10.1126/SCIENCE.1137014.
[3] L. Liu, G. Alva, X. Huang, G. Fang, Preparation, heat transfer and flow properties of microencapsulated phase change materials for thermal energy storage, Renew. Sust. Energ. Rev. 66 (2016) 399–414, https://doi.org/10.1016/J.RSER.2016.08.035.
[4] G. Abdeali, A.R. Bahramian, M. Abdollahi, Review on nanostructure supporting material strategies in shape-stabilized phase change materials, J. Energy Storage 29 (2020), 101299, https://doi.org/10.1016/J.EST.2020.101299.
[5] C. Ren, F. Liu, M.M. Umair, X. Jin, S. Zhang, B. Tang, Excellent temperature-control based on reversible thermochromic materials for light-driven phase change materials system, Molecules 24 (2019) 1623, https://doi.org/10.3390/MOLECULES24081623.
[6] Y. Zhang, M.M. Umair, S. Zhang, B. Tang, Phase change materials for electron-triggered energy conversion and storage: a review, J. Mater. Chem. A Mater. 7 (2019) 22218–22228, https://doi.org/10.1039/C9TA06678K.
[7] F. Meng, X. Zhang, R. Li, J. Zhao, X. Xuan, X. Wang, J. Zou, Q. Li, Electro-induced mechanical and thermal responses of carbon nanotube fibers, Adv. Mater. 26 (2014) 2480–2485, https://doi.org/10.1002/ADMA.201305123.
[8] G. Cheng, Z. Wang, X. Wang, Y. He, All-climate thermal management structure for batteries based on expanded graphite/polymer composite phase change material with a high thermal and electrical conductivity, Appl. Energy 322 (2022), 119509, https://doi.org/10.1016/J.APENERGY.2022.119509.
[9] R.D. Jilte, R. Kumar, M.H. Ahmadi, L. Chen, Battery thermal management system employing phase change material with cell-to-cell air cooling, Appl. Therm. Eng. 161 (2019), 114199, https://doi.org/10.1016/J.APPLTHERMALENG.2019.114199.
[10] T. Liu, S. Ge, X.G. Yang, C.Y. Wang, Effect of thermal environments on fast charging Li-ion batteries, J. Power Sources 511 (2021), 230466, https://doi.org/10.1016/J.JPOWSOUR.2021.230466.
[11] Y. Lv, X. Yang, G. Zhang, X. Li, Experimental research on the effective heating strategies for a phase change material based power battery module, Int. J. Heat Mass Transf. 128 (2019) 392–400, https://doi.org/10.1016/J.IJHEATMASSTRANSFER.2018.07.037.
[12] G. Liao, K. Jiang, F. Zhang, J.E.L. Liu, J. Chen, E. Leng, Thermal performance of battery thermal management system coupled with phase change material and thermoelectric elements, J. Energy Storage 43 (2021), 103217, https://doi.org/10.1016/J.EST.2021.103217.
[13] M. Luo, J. Song, Z. Ling, Z. Zhang, X. Fang, Phase change material coat for battery thermal management with integrated rapid heating and cooling functions from −40 °C to 50 °C, Mater. Today Energy 20 (2021), 100652, https://doi.org/10.1016/J.MTENER.2021.100652.
[14] L.W. Fan, X. Fang, X. Wang, Y. Zeng, Y.Q. Xiao, Z.T. Yu, X. Xu, Y.C. Hu, K.F. Cen, Effects of various carbon nanofillers on the thermal conductivity and energy storage properties of paraffin-based nanocomposite phase change materials, Appl. Energy 110 (2013) 163–172, https://doi.org/10.1016/J.APENERGY.2013.04.043.
[15] P. Sobolčiak, H. Abdelrazeq, N.G. Özerkan, M. Ouederni, Z. Nógellová, M. A. AlMaadeed, M. Karkri, I. Krupa, Heat transfer performance of paraffin wax based phase change materials applicable in building industry, Appl. Therm. Eng. 107 (2016) 1313–1323, https://doi.org/10.1016/J.APPLTHERMALENG.2016.07.050.
[16] T. Qian, S. Zhu, H. Wang, A. Li, B. Fan, Comparative study of single-walled carbon nanotubes and graphene nanoplatelets for improving the thermal conductivity and solar-to-light conversion of PEG-infiltrated phase-change material composites, ACS Sustain. Chem. Eng. 7 (2018) 2446–2458, https://doi.org/10.1021/ACSSUSCHEMENG.8B05335.
[17] J. Yang, L.S. Tang, R.Y. Bao, L. Bai, Z.Y. Liu, W. Yang, B.H. Xie, M.B. Yang, Largely enhanced thermal conductivity of poly (ethylene glycol)/boron nitride composite phase change materials for solar-thermal-electric energy conversion and storage with very low content of graphene nanoplatelets, Chem. Eng. J. 315 (2017) 481–490, https://doi.org/10.1016/J.CEJ.2017.01.045.
[18] J. Yang, L.-S. Tang, R.-Y. Bao, L. Bai, Z.-Y. Liu, W. Yang, B.-H. Xie, M.-B. Yang, An ice-templated assembly strategy to construct graphene oxide/boron nitride hybrid porous scaffolds in phase change materials with enhanced thermal conductivity and shape stability for light–thermal–electric energy conversion, J. Mater. Chem. A Mater. 4 (2016) 18841–18851, https://doi.org/10.1039/C6TA08454K.
[19] L. Chen, R. Zou, W. Xia, Z. Liu, Y. Shang, J. Zhu, Y. Wang, J. Lin, D. Xia, A. Cao, Electro- and photodriven phase change composites based on wax-infiltrated carbon nanotube sponges, ACS Nano 6 (2012) 10884–10892, https://doi.org/10.1021/NN304310N.
[20] L. Zhang, R. Li, B. Tang, P. Wang, Solar-thermal conversion and thermal energy storage of graphene foam-based composites, Nanoscale 8 (2016) 14600–14607, https://doi.org/10.1039/C6NR03921A.
[21] M. Maleki, H. Karimian, M. Shokouhimehr, R. Ahmadi, A. Valanezhad, A. Beitollahi, Development of graphitic domains in carbon foams for high efficient electro/photo-to-thermal energy conversion phase change composites, Chem. Eng. J. 362 (2019) 469–481, https://doi.org/10.1016/J.CEJ.2019.01.032.
[22] G. Yang, L. Zhao, C. Shen, Z. Mao, H. Xu, X. Feng, B. Wang, X. Sui, Boron nitride microsheets bridged with reduced graphene oxide as scaffolds for multifunctional shape stabilized phase change materials, Sol. Energy Mater. Sol. Cells 209 (2020), 110441, https://doi.org/10.1016/J.SOLMAT.2020.110441.
[23] P. Sobolciak, M. Karkri, M.A. Al-Maadeed, I. Krupa, Thermal characterization of phase change materials based on linear low-density polyethylene, paraffin wax and

expanded graphite, Renew.Energy 88 (2016) 372–382, https://doi.org/10.1016/J.RENENE.2015.11.056.
[24] H. Wu, S. Deng, Y. Shao, J. Yang, X. Qi, Y. Wang, Multiresponsive shape-adaptable phase change materials with cellulose nanofiber/graphene nanoplatelet hybrid-coated melamine foam for light/electro-to-thermal energy storage and utilization, ACS Appl. Mater. Interfaces 11 (2019) 46851–46863, https://doi.org/10.1021/ACSAMI.9B16612.
[25] W. Aftab, A. Mahmood, W. Guo, M. Yousaf, H. Tabassum, X. Huang, Z. Liang, A. Cao, R. Zou, Polyurethane-based flexible and conductive phase change composites for energy conversion and storage, Energy Storage Mater. 20 (2019) 401–409, https://doi.org/10.1016/J.ENSM.2018.10.014.
[26] Q. Sun, N. Zhang, H. Zhang, X. Yu, Y. Ding, Y. Yuan, Functional phase change composites with highly efficient electrical to thermal energy conversion, Renew. Energy 145 (2020) 2629–2636, https://doi.org/10.1016/J.RENENE.2019.08.007.
[27] O.M. Maithya, X. Zhu, X. Li, S.J. Korir, X. Feng, X. Sui, B. Wang, High-energy storage graphene oxide modified phase change microcapsules from regenerated chitin Pickering emulsion for photothermal conversion, Sol. Energy Mater. Sol. Cells 222 (2021), 110924, https://doi.org/10.1016/J.SOLMAT.2020.110924.
[28] Y. Zhou, X. Liu, D. Sheng, C. Lin, F. Ji, L. Dong, S. Xu, H. Wu, Y. Yang, Polyurethane-based solid-solid phase change materials with in situ reduced graphene oxide for light-thermal energy conversion and storage, Chem. Eng. J. 338 (2018) 117–125, https://doi.org/10.1016/J.CEJ.2018.01.021.
[29] X. Hu, H. Huang, Y. Hu, X. Lu, Y. Qin, Novel bio-based composite phase change materials with reduced graphene oxide-functionalized spent coffee grounds for efficient solar-to-thermal energy storage, Sol. Energy Mater. Sol. Cells 219 (2021), 110790, https://doi.org/10.1016/J.SOLMAT.2020.110790.
[30] T. Li, M. Wu, S. Wu, S. Xiang, J. Xu, J. Chao, T. Yan, T. Deng, R. Wang, Highly conductive phase change composites enabled by vertically-aligned reticulated graphite nanoplatelets for high-temperature solar photo/electro-thermal energy conversion, harvesting and storage, Nano Energy 89 (2021), 106338, https://doi.org/10.1016/J.NANOEN.2021.106338.
[31] F. Xue, Y. Lu, X.dong Qi, J.hui Yang, Y. Wang, Melamine foam-templated graphene nanoplatelet framework toward phase change materials with multiple energy conversion abilities, Chem. Eng. J. 365 (2019) 20–29, https://doi.org/10.1016/J.CEJ.2019.02.023.
[32] L. Yang, Y. Yuan, N. Zhang, Y. Dong, Y. Sun, W. Ji, Photo-to-thermal conversion and energy storage of lauric acid/expanded graphite composite phase change materials, Int. J. Energy Res. 44 (2020) 8555–8566, https://doi.org/10.1002/ER.5542.
[33] H. Tabassum, X. Huang, R. Chen, R. Zou, Tailoring thermal properties via synergistic effect in a multifunctional phase change composite based on methyl stearate, J.Materiomics 1 (2015) 229–235, https://doi.org/10.1016/J.JMAT.2015.07.002.
[34] Z. Liu, H. Wei, B. Tang, S. Xu, Z. Shufen, Novel light–driven CF/PEG/SiO2 composite phase change materials with high thermal conductivity, Sol. Energy Mater. Sol. Cells 174 (2018) 538–544, https://doi.org/10.1016/J.SOLMAT.2017.09.045.
[35] R. Agrawal, Joshua Hanna, I.Emre Gunduz, C.C. Luhrs, Epoxy–PCM composites with nanocarbons or multidimensional boron nitride as heat flow enhancers, Molecules 24 (2019) 1883, https://doi.org/10.3390/MOLECULES24101883.
[36] H. Ji, D.P. Sellan, M.T. Pettes, X. Kong, J. Ji, L. Shi, R.S. Ruoff, Enhanced thermal conductivity of phase change materials with ultrathin-graphite foams for thermal energy storage, EnergyEnviron. Sci. 7 (2014) 1185–1192, https://doi.org/10.1039/C3EE42573H.
[37] R. Wen, M. Wu, J. Zhu, S. Zhu, W. Chen, in: Preparation and characteristic of ag nanoparticle modified expanded graphite for enhancing paraffin phase change material properties 30, 2022, pp. 1046–1053, https://doi.org/10.1080/1536383X.2022.2066654.
[38] A.R. Akhiani, H.S. Cornelis Metselaar, B.C. Ang, M. Mehrali, M. Mehrali, Highly hydrophobic silanized melamine foam for facile and uniform assembly of graphene nanoplatelet towards efficient light-to-thermal energy storage, Mater. TodayEnergy 28 (2022), 101077, https://doi.org/10.1016/J.MTENER.2022.101077.
[39] W. Han, C. Ge, R. Zhang, Z. Ma, L. Wang, X. Zhang, Boron nitride foam as a polymer alternative in packaging phase change materials: synthesis, thermal properties and shape stability, Appl. Energy 238 (2019) 942–951, https://doi.org/10.1016/J.APENERGY.2019.01.153.
[40] M. Mehrali, S.Tahan Latibari, M.A. Rosen, A.Reza Akhiani, M.Sajad Naghavi, E. Sadeghinezhad, H.Simon Cornelis Metselaar, M.Mohammadi Nejad, M. Mehrali, From rice husk to high performance shape stabilized phase change materials for thermal energy storage, 2016, https://doi.org/10.1039/c6ra03721f.
[41] G. Qi J. Yang R. Bao D. Xia M. Cao W. Yang M. Yang D. Wei, Hierarchical graphene foam-based phase change materials with enhanced thermal conductivity and shape stability for efficient solar-to-thermal energy conversion and storage, (n.d.). doi: 10.1007/s12274-016-1333-1.
[42] A. Popelka, P. Sobolčiak, M. Mrlík, Z. Nogellova, I. Chodák, M. Ouederni, M.A. Al-Maadeed, I. Krupa, Foamy phase change materials based on linear low-density polyethylene and paraffin wax blends, Emergent Mater. 1 (2018) 47–54, https://doi.org/10.1007/S42247-018-0003-3.
[43] R. Chen, R. Yao, W. Xia, R. Zou, Electro/photo to heat conversion system based on polyurethane embedded graphite foam, Appl. Energy 152 (2015) 183–188, https://doi.org/10.1016/J.APENERGY.2015.01.022.
[44] J. Yang, G.Q. Qi, R.Y. Bao, K. Yi, M. Li, L. Peng, Z. Cai, M.B. Yang, D. Wei, W. Yang, Hybridizing graphene aerogel into three-dimensional graphene foam for high-performance composite phase change materials, Energy Storage Mater. 13 (2018) 88–95, https://doi.org/10.1016/J.ENSM.2017.12.028.
[45] C. Wang, L. Wang, W. Liang, F. Liu, S. Wang, H. Sun, Z. Zhu, A. Li, Enhanced light-to-thermal conversion performance of all-carbon aerogels based form-stable phase change material composites, J. Colloid Interface Sci. 605 (2022) 60–70, https://doi.org/10.1016/J.JCIS.2021.07.066.
[46] Y. Zhou, X. Wang, X. Liu, D. Sheng, F. Ji, L. Dong, S. Xu, H. Wu, Y. Yang, Polyurethane-based solid-solid phase change materials with halloysite nanotubes-hybrid graphene aerogels for efficient light- and electro-thermal conversion and storage, Carbon 142 (2019) 558–566, https://doi.org/10.1016/J.CARBON.2018.10.083. N Y.
[47] M. Karthik, A. Faik, B. D'Aguanno, Graphite foam as interpenetrating matrices for phase change paraffin wax: a candidate composite for low temperature thermal energy storage, Sol. Energy Mater. Sol. Cells 172 (2017) 324–334, https://doi.org/10.1016/J.SOLMAT.2017.08.004.
[48] X. Luo, B. Hao, H. Xiang, H. Li, Z. Tao, A novel phase change materials used for direct photothermal conversion and efficient thermal storage, Sol. Energy Mater. Sol. Cells 251 (2023), 112142, https://doi.org/10.1016/J.SOLMAT.2022.112142.
[49] M. Yang, H. Dong, K. Sun, Y. Kou, L. Zhang, J. Zhao, Y. Song, Q. Shi, Scalable synthesis of paraffin@MoS2-melamine foam composite phase change materials with superior photo-thermal conversion and storage, J. Energy Storage 56 (2022), https://doi.org/10.1016/J.EST.2022.105954.
[50] H.Y. Wu, R.T. Chen, Y.W. Shao, X.D. Qi, J.H. Yang, Y. Wang, Novel flexible phase change materials with mussel-inspired modification of melamine foam for simultaneous light-actuated shape memory and light-to-thermal energy storage capability, ACS Sustain. Chem. Eng. 7 (2019) 13532–13542, https://doi.org/10.1021/ACSSUSCHEMENG.9B03169/ASSET/IMAGES/LARGE/SC-2019-03169R_0009.JPEG.
[51] M. Liu, X. Zhang, X. Liu, X. Wu, X. Ye, J. Qiao, Z. Sun, X. Zhu, Z. Huang, Multienergy-triggered composite phase-change materials based on graphite foams synthesized from graphite extracted from spent lithium-ion batteries, ACS Sustain. Chem. Eng. 10 (2022) 8051–8063, https://doi.org/10.1021/ACSSUSCHEMENG.2C02125/ASSET/IMAGES/MEDIUM/SC2C02125_M005.GIF.
[52] P. Sobolčiak, M. Mrlik, A. Popelka, A. Minařík, M. Ilcikova, P. Srnec, Z. Nogellova, M. Ouederni, I. Krupa, Foamed phase change materials based on recycled polyethylene/paraffin wax blends, Polymers 13 (2021) 1987, https://doi.org/10.3390/POLYM13121987.
[53] W. Aftab, X. Huang, W. Wu, Z. Liang, A. Mahmood, R. Zou, Nanoconfined phase change materials for thermal energy applications, EnergyEnviron. Sci. 11 (2018) 1392–1424, https://doi.org/10.1039/C7EE03587J.
[54] W.D. Steinmann, D. Laing, R. Tamme, Development of PCM storage for process heat and power generation, in: Journal of Solar Energy Engineering, Transactions of the ASME, 131, 2009, pp. 0410091–0410094, https://doi.org/10.1115/1.3197834/447660.
[55] P. Atkin, M.M. Farid, Improving the efficiency of photovoltaic cells using PCM infused graphite and aluminium fins, Sol. Energy 114 (2015) 217–228, https://doi.org/10.1016/J.SOLENER.2015.01.037.
[56] R. Schmitt, M. Römmler, W.D. Steinmann, R. Tamme, High performance PCM-graphite heat storage systems for solar process heat, in: Proceedings of the ASME 3rd International Conference on Energy Sustainability 2009, ES2009 2, 2010, pp. 567–571, https://doi.org/10.1115/ES2009-90071.
[57] Z. Fan, Y. Zhao, X. Liu, Y. Shi, D. Jiang, Thermal properties and reliabilities of myristic acid–paraffin wax binary eutectic mixture as a phase change material for solar energy storage, RSC Adv. 12 (2022) 12303–12309, https://doi.org/10.1039/D1RA09238C.
[58] n-Nonadecanol-1 (n.d.), https://webbook.nist.gov/cgi/cbook.cgi?ID=C1454848&Type=IR-SPEC&Index=1. accessed March 27, 2023.
[59] R.A. Friedel, G.L. Carlson, Infrared spectra of ground graphite, J. Phys. Chem. 75 (1971) 1149–1151, https://doi.org/10.1021/J100678A021/ASSET/J100678A021.FP.PNG_V03.
[60] Y. Li, Y.A. Samad, K. Polychronopoulou, S.M. Alhassan, K. Liao, From biomass to high performance solar–thermal and electric–thermal energy conversion and storage materials, J. Mater. Chem. A Mater. 2 (2014) 7759–7765, https://doi.org/10.1039/C4TA00839A.
[61] C. Li, B. Zhang, Q. Liu, N-eicosane/expanded graphite as composite phase change materials for electro-driven thermal energy storage, J. Energy Storage 29 (2020), 101339, https://doi.org/10.1016/J.EST.2020.101339.
[62] W. Cui, X. Li, X. Li, T. Si, L. Lu, T. Ma, Q. Wang, Thermal performance of modified melamine foam/graphene/paraffin wax composite phase change materials for solar-thermal energy conversion and storage, J. Clean. Prod. 367 (2022), 133031.
[63] S. Xi, M. Wang, L. Wang, H. Xie, W. Yu, 3D reduced graphene oxide aerogel supported TiO2-x for shape-stable phase change composites with high photothermal efficiency and thermal conductivity, Sol. Energy Mater. Sol. Cells 226 (2021), 111068.
[64] Z. Wang, X. Zhang, Y. Xu, G. Chen, F. Lin, H. Ding, Preparation and thermal properties of shape-stabilized composite phase change materials based on paraffin wax and carbon foam, Polymer 237 (2021), 124361, https://doi.org/10.1016/J.POLYMER.2021.124361. Guildf.
[65] Y. Zhang, J. Liu, Z. Su, M. Lu, S. Liu, T. Jiang, Preparation of low-temperature composite phase change materials (C-PCMs) from modified blast furnace slag (MBFS), Constr. Build. Mater. 238 (2020), 117717, https://doi.org/10.1016/J.CONBUILDMAT.2019.117717.
[66] J. Yang, Y. Jia, N. Bing, L. Wang, H. Xie, W. Yu, Reduced graphene oxide and zirconium carbide co-modified melamine sponge/paraffin wax composites as new form-stable phase change materials for photothermal energy conversion and storage, Appl. Therm. Eng. 163 (2019), 114412, https://doi.org/10.1016/J.APPLTHERMALENG.2019.114412.

[67] G. Cheng, X. Wang, Y. He, 3D graphene paraffin composites based on sponge skeleton for photo thermal conversion and energy storage, Appl. Therm. Eng. 178 (2020), 115560, https://doi.org/10.1016/J.APPLTHERMALENG.2020.115560.
[68] F. Xue, Y. Lu, X.dong Qi, J.hui Yang, Y. Wang, Melamine foam-templated graphene nanoplatelet framework toward phase change materials with multiple energy conversion abilities, Chem. Eng. J. 365 (2019) 20–29, https://doi.org/10.1016/J.CEJ.2019.02.023.
[69] Z. Cai, J. Liu, Y. Zhou, L. Dai, H. Wang, C. Liao, X. Zou, Y. Chen, Y. Xu, Flexible phase change materials with enhanced tensile strength, thermal conductivity and photo-thermal performance, Sol. Energy Mater. Sol. Cells 219 (2021), 110728, https://doi.org/10.1016/J.SOLMAT.2020.110728.
[70] H. Zhang, L. Wang, S. Xi, H. Xie, W. Yu, 3D porous copper foam-based shape-stabilized composite phase change materials for high photothermal conversion, thermal conductivity and storage, Renew.Energy 175 (2021) 307–317, https://doi.org/10.1016/J.RENENE.2021.05.019.
[71] X. Zou, J. Liu, Polyoxyethylene based phase change materials with enhanced mechanical property, thermal conductivity and photo-thermal energy charging capacity, Energy Rep. 6 (2020) 2948–2955, https://doi.org/10.1016/J.EGYR.2020.10.022.
[72] M.M. Umair, Y. Zhang, A. Tehrim, S. Zhang, B. Tang, Form-stable phase-change composites supported by a biomass-derived carbon scaffold with multiple energy conversion abilities, cite this, Ind. Eng. Chem. Res. 59 (2020) 1393–1401, https://doi.org/10.1021/acs.iecr.9b06288.
[73] M.M. Umair, Y. Zhang, S. Zhang, X. Jin, B. Tang, A novel flexible phase change composite with electro-driven shape memory, energy conversion/storage and motion sensing properties, J. Mater. Chem. A Mater. 7 (2019) 26385–26392.
[74] Y. Li, Y.A. Samad, K. Polychronopoulou, S.M. Alhassan, K. Liao, From biomass to high performance solar–thermal and electric–thermal energy conversion and storage materials, J. Mater. Chem. A Mater. 2 (2014) 7759–7765, https://doi.org/10.1039/C4TA00839A.